Final Performance Report

High Energy Laser Multidisciplinary Research Initiative

Topic 4: High Power, Lightweight Optics

Program title: **Fabrication, Testing, Coating and Alignment of Fast Segmented Optics**

Principal Investigator: Hubert Martin

Co-Investigators: Roger Angel, James Burge, Joseph Talghader

Institution: Steward Observatory, University of Arizona, Tucson, AZ 85721

Agreement number: F49620-02-1-0384

20060619034

Summary

The Multidisciplinary Research Initiative addressed four critical technologies needed to produce large-aperture, lightweight, high-power HEL systems. They are:

1. Polishing large off-axis segments of fast primary mirrors

2. Testing large segments in an off-axis geometry

3. Alignment of multiple segments of a large mirror

4. Coatings that reflect high-intensity light without distorting the substrate

These technologies are critical because of several unique requirements that distinguish advanced HEL mirrors from other large optical systems. Future HEL systems will include mobile, deployable and space-based systems. They must combine large aperture with low weight, must be agile for rapid pointing and tracking, and must fit into a small volume for transport on the ground or in space. These requirements strongly favor segmented mirrors, which can have lower surface density than monolithic mirrors and can be packed efficiently for transport. They also favor short focal length for agility and minimum volume. The fact that the mirrors must be lightweight makes them susceptible to bending by thermal stress from a reflective coating heated by the high-power laser.

We addressed the first two technologies in the list above by extending methods of fabrication and testing that have been developed at the University of Arizona over two decades and have led to efficient production of the largest mirrors, and the most aspheric large mirrors, ever made. We extended these methods to off-axis segments of a system with short focal length, demonstrating this capability through the manufacture of a challenging 1.7 m edge segment of a 5 m f/0.7 primary mirror, a segment with 2.7 mm of asphericity. We set up a 2 m polishing machine with the stressed-lap polishing tool that is uniquely effective at figuring aspheric surface. We designed an optical test for the segment that includes a new hybrid reflective-diffractive null corrector, and built the hardware that implements this test. We used this system to polish the off-axis segment to an accuracy of $\lambda/20$ rms surface.

In addition to the hybrid null corrector for the off-axis segment, we developed two other new applications of computer-generated holograms (CGHs) to the testing and alignment of mirror segments. The first is the use of a CGH in conjunction with a spherical test plate to measure multiple segments of the same system. In addition to giving a simple and economical measurement of all the segments of an segmented mirror, this test guarantees accurate matching of the radius of curvature among all segments. The second application of CGHs is to provide references for system alignment. We pioneered the use of multiplexed holograms—holograms with multiple patterns interleaved on the same substrate—to produce reference markers for off-axis distance and rotation (clocking angle) of the segment, and reference wavefronts for alignment of the CGH to the interferometer and to other parts of the test system, as well as the reference wavefront used to measure the surface of the optic under test.

The work of our program on optical coatings concentrated on three main areas: the development of negative thermal expansion thin films, modeling the mechanical characteristics of optical coatings, and developing high power adaptive optics structures. One of the most exciting outcomes of our research is the development of the first negative thermal expansion thin films. We also determined the condition on film density for achieving negative thermal expansion. We developed a mechanical model of multilayer coatings on thin membranes and showed that it accurately predicts the deflections due to test coatings. We investigated heat transfer in micro-machined adaptive mirrors and used the results to design MEMS adaptive mirrors with enhanced heat transfer and very long throw.

The results of this research program will reduce the cost and manufacturing time for large, lightweight HEL mirrors, and improve their performance.

1. Introduction

Optical systems for high-energy laser projection have unique requirements that set them apart from conventional optical systems. They must have large apertures in order to maximize laser power without unacceptable intensity on the mirror surface. They need to be agile, mobile and deployable, and some will be based in space. Large apertures must therefore be combined with low weight. Both the requirement for lightweight mirrors and the need for transport and deployment strongly favor segmented mirrors. Short focal length is also favored for maximum agility and minimum volume.

Optics that meet these requirements strain current manufacturing capabilities in several ways. While segments, including off-axis segments, have been made for a number of telescopes, their manufacture is costly and inefficient. Methods of making off-axis aspheres need to be improved to approach the efficiency with which spherical surfaces can be mass-produced. They must also be extended to handle the more extreme aspheres of large mirrors with short focal lengths. This requires advances in both fabrication (primarily polishing) and testing. These techniques must be applicable to lightweight mirrors with little intrinsic stiffness. In this Multidisciplinary Research Initiative (MRI) we used a technique that has been proven to work efficiently and accurately on axisymmetric aspheric surfaces, and demonstrated its efficiency for off-axis aspheres.

In order to synthesize a large aperture out of many segments, we need ways to maintain a consistent geometry, especially radius of curvature, among segments. And we need ways to control alignment of the segments during manufacture and during operation. These requirements for radius matching and alignment are more demanding as the focal length decreases. Conventional metrology with reflective or refractive test optics (including null lenses) has large uncertainties for highly aspheric, asymmetric surfaces and leaves ambiguities in radius of curvature and alignment. These limitations can be eliminated through the use of a computer-generated hologram (CGH). In this MRI we pushed holographic techniques into new areas and to new levels of accuracy.

Finally, large, lightweight optics used with high-energy lasers are highly susceptible to bending due to thermal stress in the coatings. While designers know a great deal about the optical properties of coatings, less is known about their mechanical and thermal properties and how they interact with the substrate, and even what *is* known is not used to full advantage. We built and experimentally verified a mechanical model of multi-layer coatings that allows a designer to optimize for thermal and mechanical properties as well as optical properties. We also significantly expanded the range of thermo-elastic properties available, by depositing the first thin film with a negative thermal expansion coefficient.

2. Highlights of the MRI

The major accomplishments of the MRI are as follows:

1. Preparation of a 2 m stressed-lap polishing system capable of figuring an off-axis segment of a fast (f/0.7) parent paraboloid.

2. Manufacture of a high-quality 1.7 m off-axis mirror segment accurate to $\lambda/20$ rms surface.

3. Designing and building a hybrid reflective-diffractive optical system capable of measuring the off-axis segment to high accuracy, both its surface figure and its alignment.

4. Developing a new measurement technique combining a traditional test plate and a CGH, that can be used to measure all the segments of a segmented mirror, including tight control of radius of curvature and alignment.

5. Designing and demonstrating the use of multiplexed holograms that combine reference wavefronts for figure testing with powerful alignment tools.

6. The first deposition of a thin film with negative thermal expansion, and determination of conditions that allow the negative expansion behavior.

7. Development of a thermal and mechanical model of multi-layer coatings, and experimental verification of the model.

8. Design and initial processing of MEMS adaptive mirrors with enhanced heat transfer and very long throw.

These highlights, as well as other developments, are discussed in more detail in the remainder of this report.

3. Figuring large off-axis segments to the diffraction limit

One of the central goals of the MRI was the manufacture of an off-axis mirror segment that could be part of a large segmented optical system. We selected a 1.7 m segment of a 5.3 m f/0.7 parent paraboloid. We extended a polishing process that we have proven to be efficient and accurate through the manufacture of ten highly aspheric symmetric mirrors with diameters between 1.8 m and 8.4 m. At the heart of the process is an actively stressed lap (polishing tool) that bends dynamically under computer control to match the local curvature of the aspheric optical surface at all times. We extended this process to the asymmetric surface of the off-axis segment.

3.1 Design and preparation of the polishing system

The first step in this process was the preparation of a 2 m polishing machine with a 30 cm diameter stressed lap. The machine was used previously in a different facility. We installed it in a new lab that can accommodate both the polishing machine and the test tower for the off-axis mirror. Figure 1 shows the machine in its new location along with a close-up view of the stressed lap. We analyzed the bending capacity of the stressed lap to confirm that it can bend enough to follow the 2.7 mm asphericity of the off-axis segment. This is 10 times greater asphericity than we have encountered in axisymmetric mirrors, but because most of the asphericity is low-order (astigmatism) the lap can accommodate it.
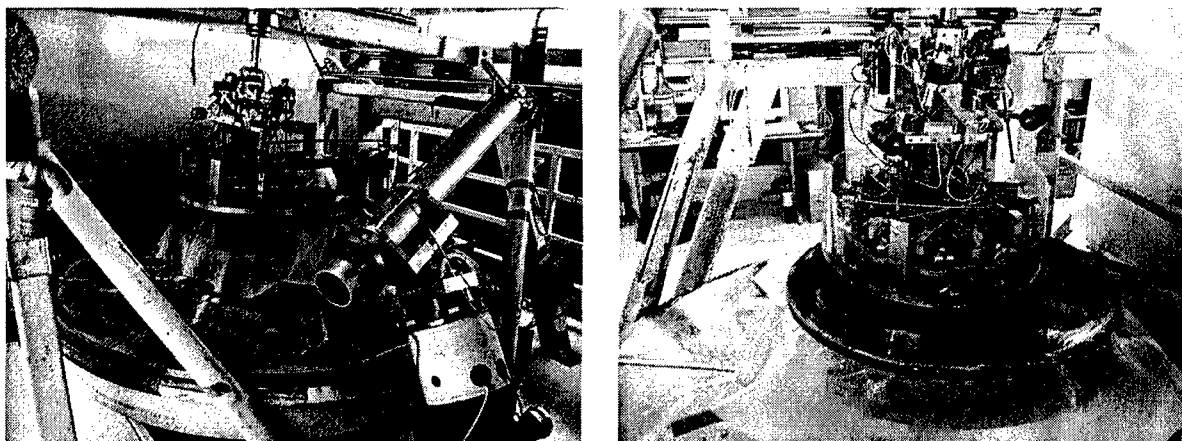

Figure 1. Stressed-lap polishing machine that will be used to figure the 1.7 m off-axis segment. The 30 cm stressed lap is shown polishing a 0.9 m mirror.

The mirror being polished in Figure 1 is the first of two adaptive secondary mirrors for the 2 x 8.4 m Large Binocular Telescope (LBT)—prior commitments that had to be completed before we polish the off-axis segment. These mirrors are the secondary mirrors for the world's largest telescope *and* the deformable mirrors of its adaptive optics system. They are made using a method developed at the Mirror Lab in which a thick, stiff mirror is figured to a smooth surface (very accurate on small scales, while large

scales are less important), and later thinned to give it the weight and flexibility needed to correct the atmosphere with kHz response. The same technique is applicable to lightweight segments of a large, segmented HEL mirror. The final thickness of the LBT secondaries is 1.6 mm. We experienced several delays in the production of this first LBT secondary but used the experience to make the polishing system more reliable and refine the figuring techniques. This mirror was completed to high accuracy—10 nm rms surface error after simulated correction with its 672 actuators—in September 2004. A second, identical mirror was completed in December 2004.

3.2 Fabrication of the segment

For the off-axis mirror segment, a 100 mm thick Zerodur mirror blank was purchased from Schott. Figure 2 shows the segment and its support for polishing and testing in the lab. We optimized the mirror support geometry with a finite-element model, constraining all 36 supports to equal force for simplicity. The optimized support reduces self-weight deflections to 5 nm rms.
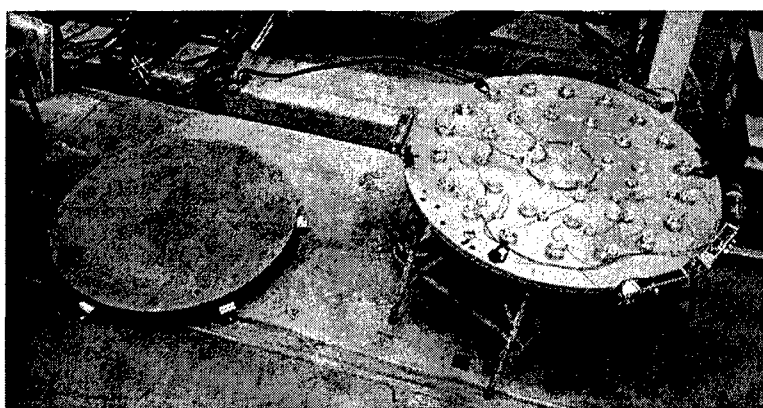

Figure 2. The 1.7 m mirror at left, with its 36 point support that will be used for polishing and testing.

The aspheric surface was generated to an accuracy of about 15 μm rms by ITT Industries. Loose-abrasive grinding and polishing were performed by the Mirror Lab. We polished the mirror primarily using a 30 cm diameter stressed lap, essentially the same system used to polish the 1.8 m f/1 primary mirror of the Vatican Advanced Technology Telescope and secondary mirrors for the 3.5 m ARC telescope, 2.5 m Sloan Digital Sky Survey telescope, MMT (three secondaries) and the Large Binocular Telescope (two secondaries). The stressed lap changes shape actively to follow the local curvature of the mirror surface. It consists of a 13 mm thick aluminum plate with actuators around its perimeter that apply bending and twisting moments. The plate is stiff enough to provide strong passive smoothing of errors with periods less than about 100 mm. Errors on larger scales are addressed by varying the lap's dwell time, rotation rate, and pressure. This method is augmented by local polishing with passive laps of 50-100 mm diameter.

The stressed-lap polishing system works equally well for axisymmetric and non-axisymmetric mirrors. The lap's ability to polish a given surface depends on the amount it has to bend in order to follow the curvature variations of that surface. The asphericity of the off-axis segment has a large amplitude but is dominated by astigmatism and coma, which have relatively small curvature variations, as shown in Figure 3. The required bending of the lap is only about 5% of the full amplitude of asphericity, a much lower ratio than would apply to an axisymmetric mirror whose asphericity is spherical aberration. The lap bending required for the off-axis segment is less than the bending required for several of the secondary mirrors that have been figured to high accuracy using the same lap.
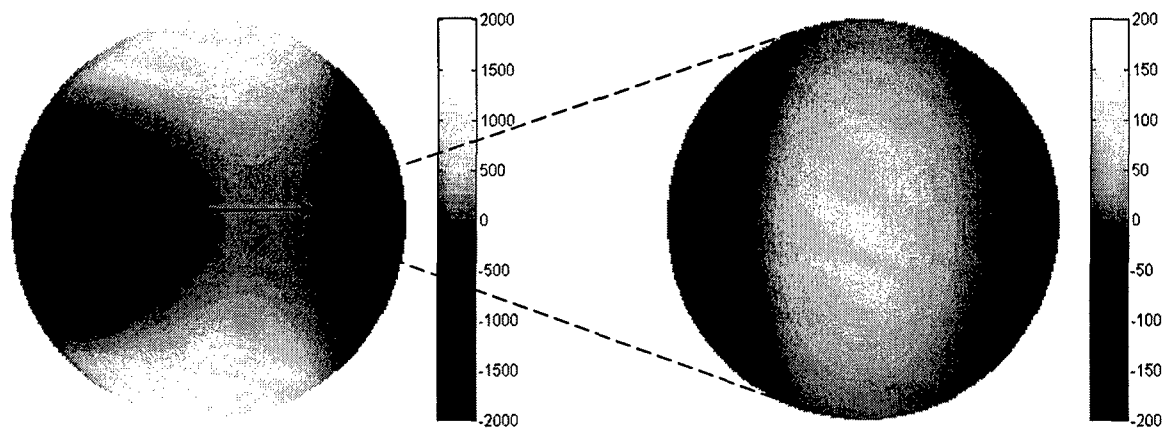
Figure 3. Representation of the asphericity of the 1.7 m off-axis mirror segment (left), and the bending of the 30 cm stressed lap as it moves from one edge of the segment to the opposite edge (right). Color bars are labeled in μm; note the factor-of-ten difference in scales.

We used the stressed lap for loose-abrasive grinding in order to remove subsurface damage and improve the figure accuracy to about 1 μm rms surface. During this phase we measured the surface with a laser tracker as described below. We then polished and figured the surface with the stressed lap and small passive tools. During both loose-abrasive grinding and polishing, we figured the mirror using the same type of polishing strokes that would be used for an axisymmetric mirror. The lack of symmetry in the surface is taken up entirely by the bending of the stressed lap, with an amplitude of only a few hundred μm as seen in Figure 3. An observer would not discern that the mirror being polished is off-axis.

Figure 4 shows two views of the off-axis segment. The photo at left shows the segment shortly after delivery from ITT. We bonded 36 invar pucks to the rear surface to interface to an active support system in a telescope as well as the passive polishing support seen in the photo. Before polishing began, we developed techniques and software to measure the surface with the laser tracker. The photo at right shows the segment being polished.
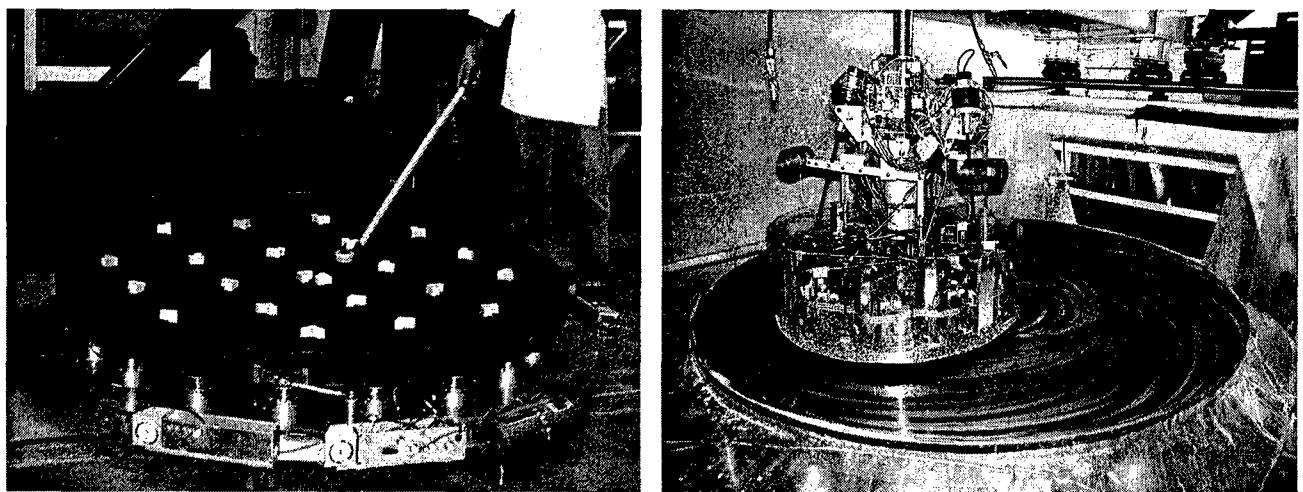

Figure 4. Two views of the off-axis segment. Left: resting on its polishing support, before polishing, while a technician practices measuring the surface with a laser tracker. Right: being polished with the 30 cm stressed lap.

3.3 Surface measurements with a laser tracker

For symmetric mirrors up to 2 m in diameter, we measure the ground surface with a swing-arm profilometer that makes a one-dimensional scan roughly across a diameter of the mirror. The profilometer can measure asphericity to an accuracy of about 50 nm rms, but it is relatively insensitive to average curvature (power). For the off-axis segment, the profilometer cannot measure the difference in sag between the two orthogonal diameters (46.0 mm vs 43.5 mm) to an accuracy of a few μm, as is needed to make the transition from loose-abrasive grinding to polishing and testing at 633 nm.

We decided to measure the ground surface with a commercial laser tracker, which combines a distance-measuring interferometer with angular encoders and servos so that it can track a moving retroreflector and measure its position in three dimensions. The retroreflector is mounted in a steel ball with its vertex near the center of the ball, so the tracker measures to a point at a fixed distance (the ball radius) away from any surface. The distance-measuring interferometer measures displacements of a fraction of a μm, but the advertised accuracy of the angular encoders is about 1 arcsecond. This would correspond to a position error of about 10 μm over the roughly 2 m distance required to measure the surface of the off-axis segment. If the tracker is placed near the mirror's center of curvature, however, the measurement is not very sensitive to angular errors.

We tested three commercial trackers by measuring the figure of a 1.8 m spherical mirror with $R = 10$ m, from its center of curvature. All three showed the surface to be accurate to less than 2 μm rms, which means the trackers were accurate to better than 2 μm rms in this favorable geometry. Furthermore, we found that the accuracy was not degraded significantly by moving the tracker to a distance of 3 m from the mirror. (This distance results in a maximum angle of incidence of 12° for the tracker beam at the edge of the mirror, and an apparent surface error of about 3 μm for a 1 arcsecond angular error.)

We purchased a tracker and developed procedures for measuring the surface of the off-axis segment, initially in the lab before starting the loose-abrasive grinding. The basic procedure is to place the tracker ball at different points on the mirror surface and measure their positions. Our initial plan was to fit a paraboloidal surface to these points and determine both the best-fit geometry of the off-axis paraboloid (radius of curvature, off-axis distance and clocking angle) and the departure from the best-fit surface. We found that a better method is to hold the off-axis distance and clocking angle fixed (constrained by measurement of fiducial points at known locations on the segment) and measure the surface error with respect to the ideal paraboloidal surface. Errors in the geometry are equivalent to low-order aberrations in the optical surface. Table 1 lists the sensitivity of each low-order aberration to errors in geometry. If the segment geometry is held fixed—i. e., the segment is constrained to be at the correct off-axis distance and clocking angle, and the radius of curvature is not allowed to vary—we simply measure these aberrations in the surface and treat them as errors to be corrected. This method was preferred especially for loose-abrasive grinding, when we could remove enough glass to correct the aberrations that correspond to errors in the geometry. Later, when we were polishing the mirror and making optical measurements, we did not constrain the mirror's position but adjusted it to minimize the low-order aberrations. We did, however, monitor the segment's position as described below.

7

Table 1. Sensitivity of low-order aberrations to errors in segment geometry. Aberrations are given as Zernike polynomial coefficients in μm, with polynomials normalized to unit rms surface error.

	focus	astigmatism (0°)	astigmatism (45°)	coma (0°)	coma (90°)
radius of curvature: +1 mm	-1.76	0	0	0	0
off-axis distance: +1 mm	0.84	0.60	0	0.08	0
clocking: 1.2 mrad = 1 mm counterclockwise	0	0	-1.3	0	-0.17

We built a small fixture to hold the tracker ball at a fixed distance from the edge of the segment and a fixed distance from the optical surface, at four positions at 90° intervals around the edge of the segment. We know the positions of these four fiducial points in a coordinate system centered on the mechanical center of the segment. By a coordinate transformation we know their positions in a coordinate system centered on the vertex of the parent paraboloid, assuming the segment has the correct radius of curvature, off-axis distance and clocking angle. Each scan includes measurements of these four points and a series of at least 100 points on the mirror surface. Sampling the surface takes about 5 minutes in continuous measurement mode (see below) or 10 minutes for stop-and-go measurements. Data are recorded in the tracker's native coordinate system, but any coordinate system would do.

To process the data, we first use the four fiducial points to find the transformation from measured coordinates to parent coordinates, i. e. the transformation that puts these four points at the correct positions in the parent coordinates. Using four points provides some redundancy, giving a least-squares solution and an indication of a significant error in any of the four points. Typical residual errors after the best-fit transformation are on the order of 0.2 mm, consistent with the uncertainty in placing the ball on the mirror. This is more than adequate to define the off-axis distance and clocking angle but not to define the piston, tip and tilt of the surface, so these parameters are allowed to float when the surface data are processed.

Next, we take the coordinate transformation obtained from the four fiducial points and apply it to the surface data, thereby putting the surface data in the parent coordinate system. We then find the departure of each point from the ideal surface. The data contain errors on the order of 100 μm in the form of piston, tip and tilt because of errors in the positions of the fiducial points, and these are ignored. We fit Zernike polynomials to the residual errors, typically using polynomials through 6th degree in radius, and take this polynomial fit as the best representation of the surface.

The tracker can measure on command, taking a single sample or an average of multiple samples of a stationary retroreflector. It can also measure as the retroreflector moves continuously, triggering its own measurements according to a user-defined distance between samples. We found that either method works well for a ground surface. The continuous method requires dragging the steel ball over the surface, and this turned out to be the simplest method for the ground surface. We built a wand, seen in Figure 4, that allows a technician to move the ball over the surface without deflecting the segment. We also used the laser tracker in the early stages of polishing before the surface was specular enough for the interferometric measurement. For the polished surface we measured at discrete points with the ball stationary, and modified the wand to include a plastic shield that could be inserted between the ball and the mirror surface when we moved from point to point. We took care never to hold the steel ball over the segment without having protection in place.

The segment remains on the polishing turntable for the tracker measurements. The tracker is mounted about 2 m above the mirror on a bridge that is locked in place for each measurement. This arrangement is shown in Figure 5 for a different mirror. We found, by rotating the mirror to different

orientations, that the tracker has systematic errors that appear as astigmatism in the mirror surface. This may be related to the fact that we could not perform the recommended calibration measurements with the tracker mounted over the segment, due to space constraints. We therefore routinely made two measurements, with the segment rotated 90° between them, in order to average out the astigmatic error.
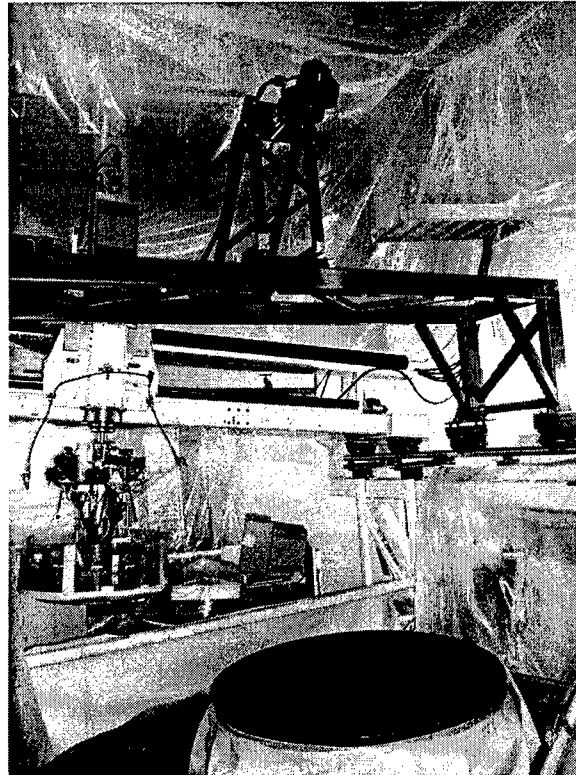

Figure 5. Laser tracker mounted over a 1 m mirror. The same arrangement was used for the 1.7 m off-axis segment.

The tracker measurements guided the loose-abrasive grinding and initial polishing from a measured error of 14 μm rms surface to a measured error of 0.9 μm rms (0.6 μm rms with focus removed). Figure 6 shows tracker data taken near the beginning of loose-abrasive grinding and near the end. The astigmatism in the early measurement was repeatable and was gradually reduced through figuring, using dynamic variations of grinding pressure. All measurements include some power, which was treated as a real error to be corrected by figuring. By the end of loose-abrasive grinding, non-repeatable noise contributed 1-2 μm rms to the measured errors. This noise was eliminated in the polynomial fits that guided the figuring.

The purpose of the tracker measurements was to guide the figuring to an accuracy that would allow optical testing. The first optical measurement easily resolved fringes at 633 nm and is in good agreement with the tracker measurement, as shown in Figure 7. The interferogram at the lower left shows the excellent contrast of the data, the severe distortion caused by the null corrector, and the accuracy of the mirror surface after figuring solely on the basis of laser tracker measurements. Focus, astigmatism and coma are strongly affected by alignment of the segment in the optical test; with these aberrations removed, the difference between the optical measurement and the polynomial fit to the tracker measurement was 0.5 μm rms surface.
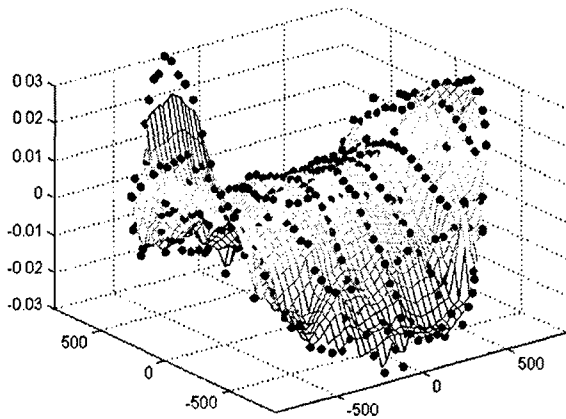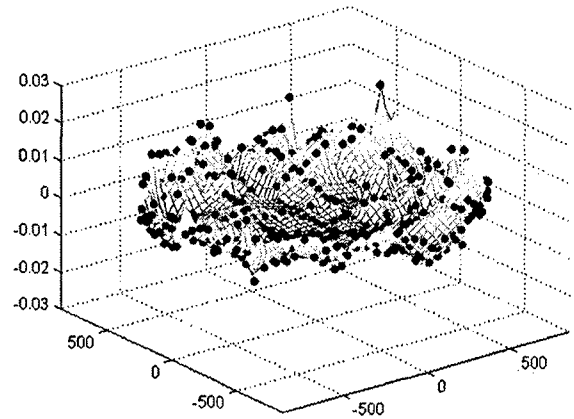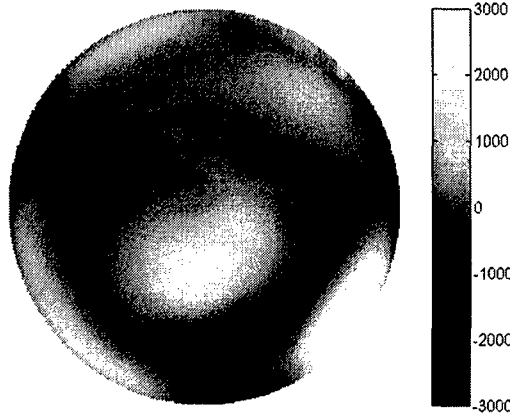
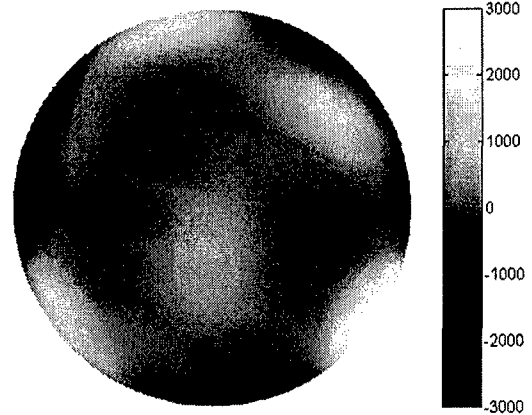31 March 2005: 14 um rms surface   22 April 2005: 4 um rms surface
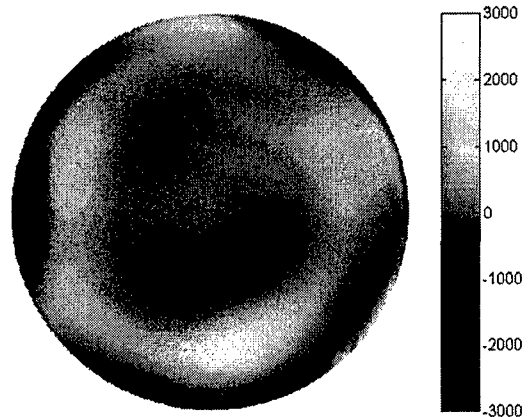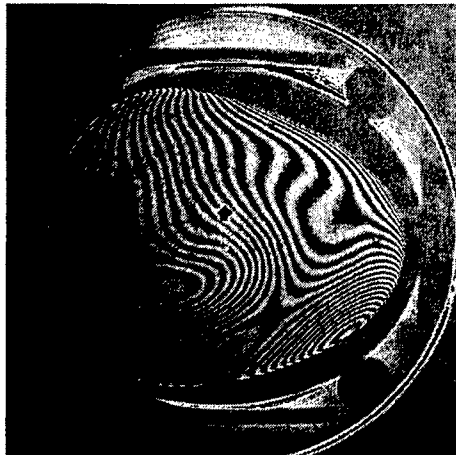
Figure 6. Laser tracker measurements of the off-axis mirror surface near the beginning of loose-abrasive grinding and near the end. The plots show the departure from the ideal off-axis paraboloid, in mm, with only piston, tip and tilt removed.

optical measurement: 630 nm rms surface   tracker measurement: 590 nm rms surface

tracker - optical: 520 nm rms surface

Figure 7. Comparison of one of the first optical measurements (two images at left) with laser tracker data taken at the same time (upper right). The difference is shown at lower right. The tracker map is a 6th-degree Zernike polynomial fit to data such as those shown in Figure 4. Focus, coma and astigmatism, which depend strongly on the alignment of the mirror in the optical test, were removed from all three maps. Color bars are labeled in nm of surface.

10

3.4 Status of the 1.7 m off-axis mirror segment

We continued to polish the mirror , guided by measurements with an optical interferometer as described in Section 4.2. The surface figure of the off-axis segment as measured in December 2005 is shown in Figure 8. The measurements show 32 nm rms after removal of some low-order aberrations that will be controlled by the active supports. Further improvement is expected as we continue to polish the surface.
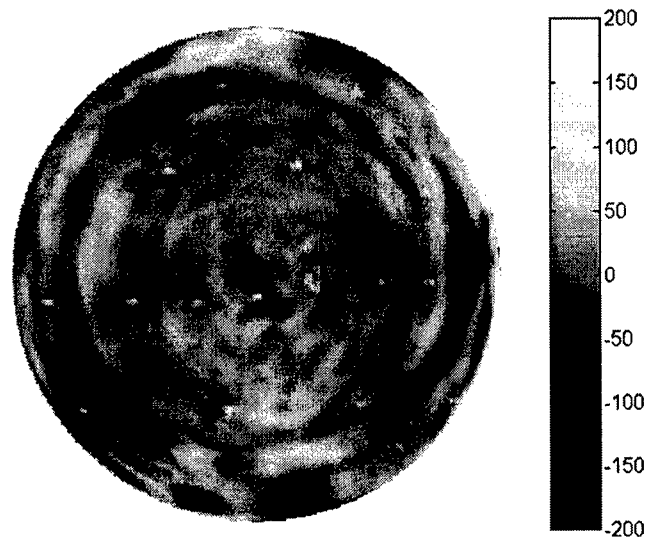

Figure 8. Figure of the off-axis segment as of December 2005. Only a 1.6 m clear aperture is shown. Small amounts of low-order aberrations that would be corrected by an active support system have been subtracted. The rms surface error is 32 nm. The color bar is labeled in nm of surface error.

4. Metrology for HEL optics using computer-generated holograms

Our program was initiated to develop concepts for measuring and aligning large highly aspheric mirrors, such as those used in laser beam projectors. The MRI is supporting three overlapping initiatives in metrology, pushing the state of the art in CGHs.:

1. **CGH with test plate for measuring mirror segments**
    This powerful new technology enables efficient and accurate measurement of segments of an aspheric mirror. The key innovation is the use of a spherical reference surface held near the mirror under test, which enables the accurate curvature measurements necessary for large segmented optics. The aspheric departure of the segment under test is compensated using a small CGH placed elsewhere in the optical train. A prototype system was successfully developed and tested. Complete system design and analysis were performed to optimize this test method for economically measuring the entire set of segments for a large fast primary mirror.

2. **Using CGH for surface metrology of large off-axis mirrors**
    We designed, built and demonstrated an optical system to measure the 1.7 m off-axis parabola. The system was specifically designed to be scalable to larger or steeper mirrors. This ambitious system relies on the alignment techniques discussed below.

3. **Using CGH to provide reference for system alignment**
    We have pioneered the use of multiplexed holograms—holograms with multiple patterns interleaved on the same substrate—for use as alignment tools. We validated our analysis in prototype

experiments and we implemented this powerful new technology into the hardware for measuring the 1.7 m segment.

4.1 CGH with test plate for measuring mirror segments

We have successfully developed and proven a method that is optimal for measuring mirror segments using a test plate and CGH. This technique is ideally suited to the measurement of primary mirror segments because the radius of curvature is closely controlled, and it allows economic, efficient testing of the segments from different parts of the primary.

Using this measurement technique, general aspheric surfaces are measured using spherical test plates with CGHs. The spherical surface creates a reference wavefront for interferometric measurement, and a small hologram is elsewhere in the system to correct the aspheric departure of the light reflected from the part under test. This allows a null test with the light from a well-known sphere as the reference. This test has several important advantages over other techniques, including the following:

- High accuracy: Using holograms fabricated by electron beam lithography, this test can achieve accuracy of $\lambda/100$ for large, steep, off-axis aspheres.

- Low cost: This test requires only one highly accurate surface—the reference spherical surface of the test plate. The other optics and the holograms need only be made to standard shop tolerances.

- Easy to implement: The reference surface is nearly coincident with the mirror surface, so the other optics do not directly affect the measurement. The absence of measurement noise due to vibration and seeing allows extremely efficient optical testing.

- Allows accurate radius measurement: The measurement of the radius of curvature is limited only by the ability to measure the small gap between the optic and the test plate. We have demonstrated the importance of this matching for mirror segments that must fit together. This work was published in *Applied Optics*.

- Allows accurate determination of axis location: Features on the hologram can be used to allow absolute lateral alignment of the asphere in the test.

This test of a concave mirror surface uses a spherical convex reference surface held in close proximity to the mirror being measured. By controlling the gap between the test plate and the mirror segment, the radius of curvature can be controlled to very high accuracy. The basic geometry is shown below in Figure 9. The important feature of this design is the CGH, which pre-distorts the test wavefront so that, after reflecting off the aspheric mirror segment, it matches the spherical reference wavefront. Both reference and test beams go through the CGH and the test plate together, so the refractive index variations and surface figures of the CGH substrate are not important. The test wavefront uses the first order of diffraction and the reference wave uses the 0-order. The fact that the wavefronts are coincident at the CGH is important because it allows the CGH to be written on a standard lithography substrate and it allows the test plate to be made from a non-precision transmission grade glass, like Zerodur.
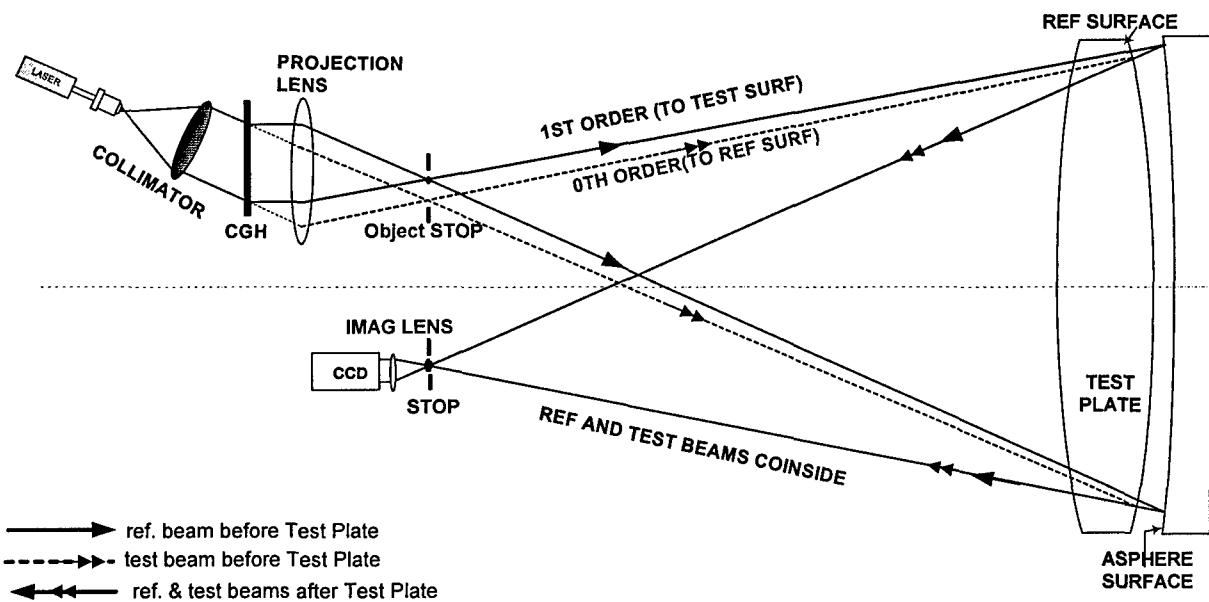
Figure 9. Layout of CGH test where hologram is imaged to test surface. The first and zero orders from the CGH are projected using the projection lens so that a good image of the CGH is formed on the test part. The hologram is designed so the 1ˢᵗ-order light reflected from the segment will exactly match the 0-order light reflected from the test plate. The other reflections are blocked. An imaging lens is used to focus the interferogram onto a CCD array.

The test achieves high accuracy using CGHs written using electron beam or direct-write laser lithography, which were developed for manufacturing integrated circuits. For nominal line space of 20 μm, holograms with pattern accuracy of 0.125 μm give 0.006 λ accuracy in the wavefront, or 0.003 λ in the surface.

This method was demonstrated using 30 cm optics, as shown in Figure 10, which shows the test plate and mirror under test, along with a snapshot of the interference fringes. The data from the test were outstanding. We proved that such a simple system can be used for measuring general surfaces to an accuracy of λ/100 rms. Figure 11 shows a comparison of the measurement of a 30 cm mirror using the new CGH method alongside the measurement with a conventional method. The residual error of noise and low order alignment errors fit within our expectations based on the error analysis. This work was accepted for publication in *Applied Optics*.
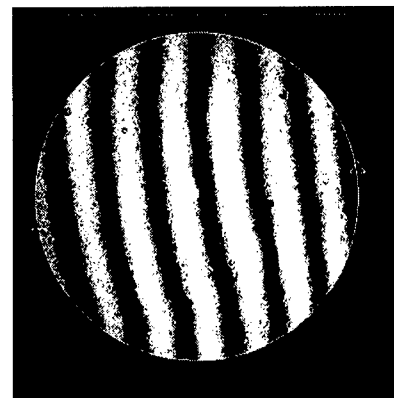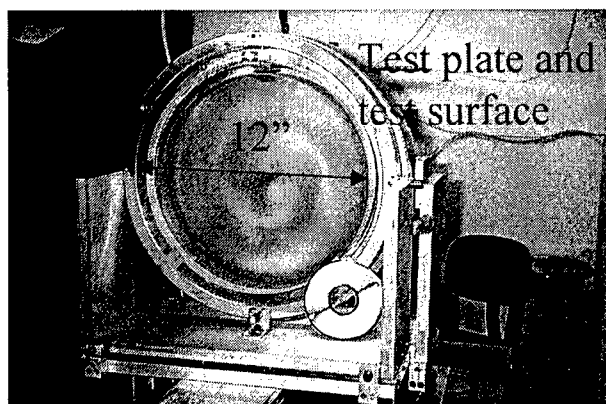
Figure 10. The optical test using a CGH and test plate was successfully demonstrated using 30 cm optics. The prototype system proved the concept of using different orders of diffraction from the same CGH to control the amplitude and phase of both wavefronts in the measurement system.

Conventional measurement	Measurement using Test plate with CGH	Difference
0.055 λ rms	0.049 λ rms	0.012 λ rms
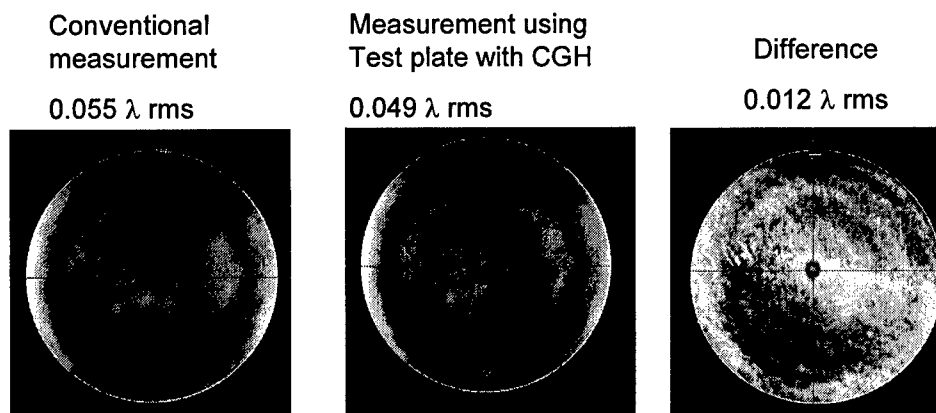
The difference of 0.012 λ rms is made up from
    0.009 λ rms low order, expected from alignment tolerances
    0.007 λ rms, looks like coherence noise

Figure 11. Successful demonstration of CGH with test plate for measuring a 30 cm concave mirror.

We have since been working with industry to provide this technology for mirror segments for a proposed 30 m telescope. We performed a complete system design and error analysis, including a trade study that investigated the cost vs performance for the holograms for this test. This work was accepted for publication in *Applied Optics*.

4.2 Using a CGH for surface metrology

We designed, built and demonstrated the system for measuring the 1.7 m off-axis segment. The basic concept of this system uses an interferometer with a null corrector that compensates for the aspheric departure of the mirror. Conventional null correctors are not practical for such large aspheric, off-axis mirrors. We use a combination of CGH and tilted mirror, where the CGH provides alignment information as well as wavefront correction. Figure 12 shows the configuration of the test. Figure 13 shows some of the important hardware. This test makes use of the technology developed under this program for aligning complex optical systems. The details are given in Section 4.3.
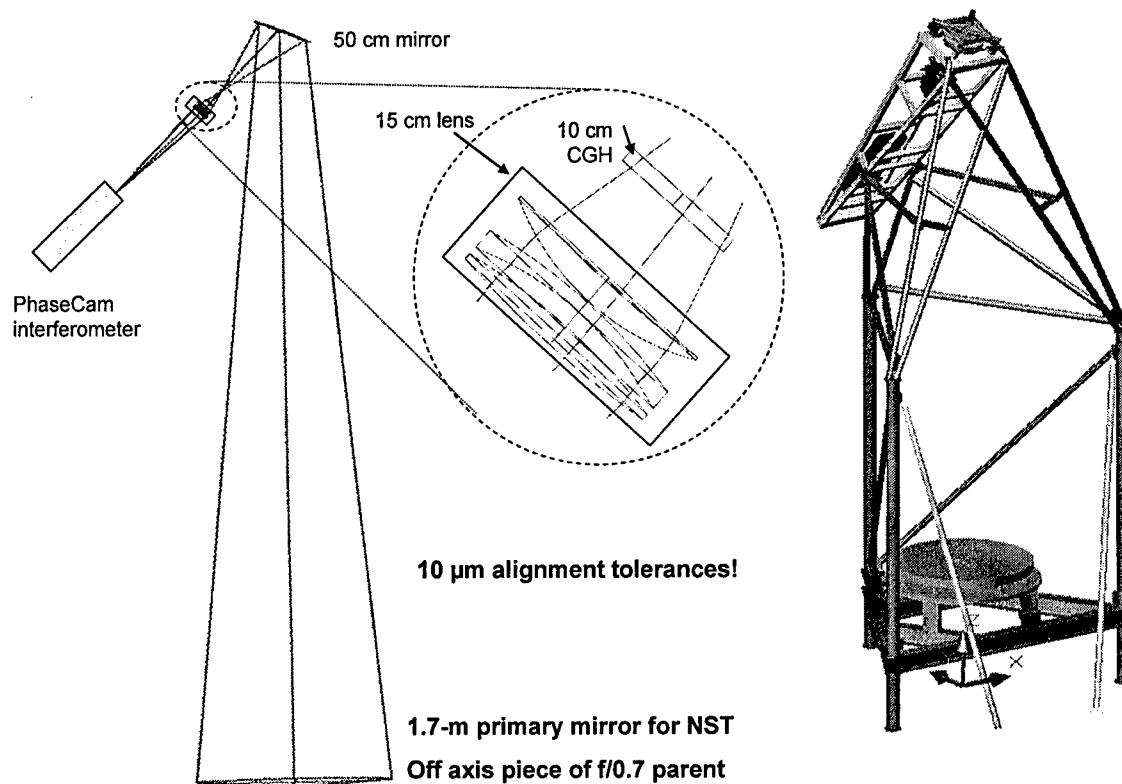
50 cm mirror

15 cm lens

10 cm
CGH

PhaseCam
interferometer

10 µm alignment tolerances!

1.7-m primary mirror for NST

Off axis piece of f/0.7 parent

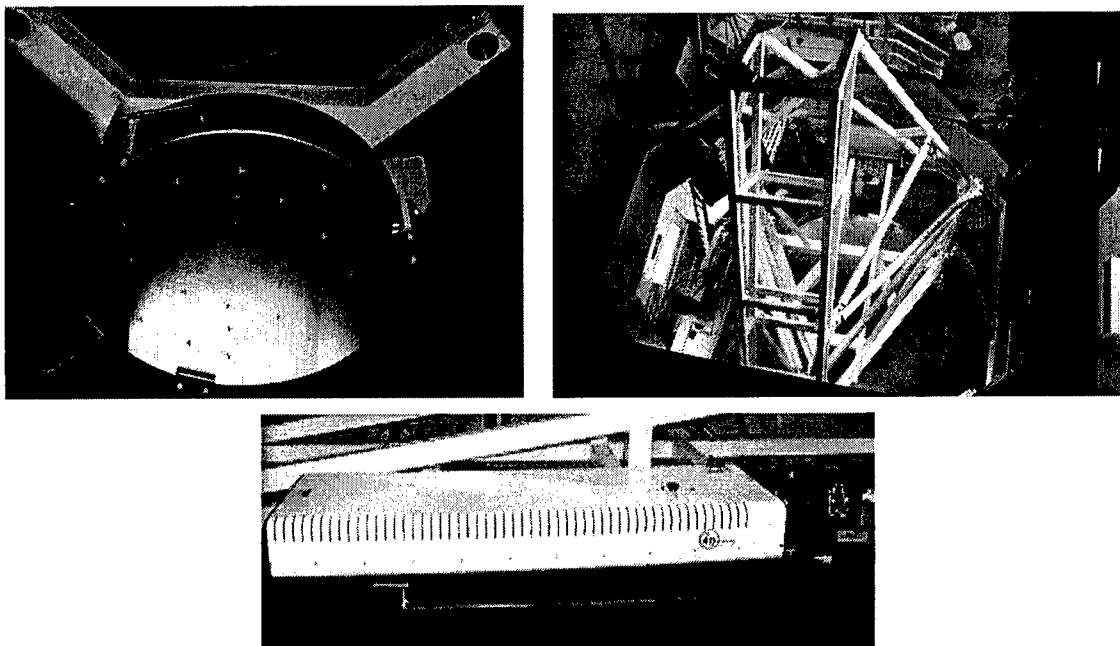**Figure 12. Optical layout and mechanical design for the optical test of the 1.7-m off-axis asphere.**

Figure 13. Key components of the metrology system for the 1.7 m segment. Clockwise from upper left: 0.5 m spherical mirror, test tower, interferometer.

15

Alignment of the components of the test is critical. The tolerance analysis for alignment is based on the fact that the segment will be aligned in the beam projector to optimize its reflected wavefront, then several low-order aberrations will be corrected by the lightweight segment's active support system. The tolerance analysis simulates this procedure as follows. For each alignment parameter in turn:

1. The parameter is perturbed, causing a wavefront error that would be imprinted on the surface of the segment.

2. The alignment of the segment in the beam projector is adjusted (in the ray-trace program) to compensate for this wavefront error.

3. Support forces are optimized to minimize the remaining wavefront error.

A more precise statement of step 2 is that the alignment of the segment is adjusted to minimize the support forces required to correct the wavefront error remaining after realignment. For example, to correct one wave of coma by bending the segment requires much larger forces than those required to correct one wave of astigmatism. Therefore coma is weighted more heavily than astigmatism in step 2. Optimization of support forces in step 3 uses only low-order bending modes that nearly match the low-order optical aberrations. The bending modes and corresponding actuator forces are calculated from a finite-element model of the mirror segment.

The tolerance analysis keeps track of the displacement of the segment from its nominal alignment, the support forces used to correct the residual error after realignment, and the remaining wavefront error after applying the support forces. Table 2 shows the results of this analysis. We are confident that the techniques described in Section 4.3 will ensure that the misalignments of the components are less than the values used for Table 2. As shown in Table 2, the effect of alignment errors in the test optics is expected to be a change in off-axis distance by less than 0.5 mm, a clocking of less than 0.1 mrad, correction forces less than 14 N rms, and a residual wavefront error less than 24 nm.

Table 2. Tolerance analysis for alignment of the components of the optical test. The interferometer is the reference for displacements of the components. Tilts are expressed as displacement at the edge of the component.

Component	parameter	tolerance	radial shift compensation	clocking compensation	rms correction force	rms wavefront error
		μm	mm	mrad	N	nm
hologram (100 mm diameter)	axial position	10	0.00	0.00	6.4	5.5
	tilt in x	50	0.01	0.01	5.0	10.9
	tilt in y	50	0.01	0.01	3.0	6.4
spherical mirror (500 mm diameter)	axial position	10	0.17	0	2.0	5.2
	tilt in x	10	0.21	0	6.4	8.4
	tilt in y	10	0	0.09	2.1	2.1
	radius of curvature	100	0.25	0	6.2	9.0
temperature		1 K	0.29	0	5.4	13.5
net change (sum in quadrature)			0.46	0.09	13.9	23.5

4.3 Using a CGH to provide reference for system alignment

We made a major breakthrough by coupling multiplexed CGHs with direct mechanical measurements for aligning complex optical systems. There are four types of CGH that we use simultaneously:

1. Alignment reference CGH. This gives return wavefront signal that is used as the reference to align the CGH to an interferometer.

2. Wavefront measurement CGH. This allow us to measure the surface of a mirror or lens.

3. Holographic alignment pattern. This uses diffraction to project light so that it focuses into a neat crosshair. This is used for alignment of lateral position.

4. Tooling ball reference. This gives a wavefront that is used to define the position of a tooling ball.

We can define many different degrees of freedom with a single multiplexed CGH.

We fully developed the concept of creating holographic reference marks and using them to position aspheric optical components. Figure 14 shows such an alignment mark that was used for positioning a 50 cm off-axis parabola. We have demonstrated that this concept can provide position information that is accurate to 10 μm.

The alignment references described above give accurate information for the lateral position of optical components, but to do not provide accurate information on axial dimensions. We have combined the power and flexibility of using CGH references with axial metrology that uses interferometry as a standard. We use the multiplexed hologram to provide the information about the lateral position for tooling balls (precision metal spheres) and we use direct mechanical measurements to set the spacing between the balls. This fully constrains all degrees of freedom and the method can work to accuracy of a few microns over several meters.

We implemented this technology for the alignment of the test optics for the 1.7 m segment. Figure 15 shows how the light is used to define the position of a reference sphere, where the zero-order diffraction light focuses, and an array of tooling balls that are fixed to the 50 cm spherical mirror for the test. The distance between the reference sphere and the spheres on the mirror is measured using metering rods that were calibrated with distance measuring interferometry. This alignment technique is extremely accurate and flexible for applications for just about any optical system. Figure 16 shows the patterns on the multiplexed CGH.

These patterns create reference marks at any desired location.

Locate pattern visually or with calibrated CCD and transfer to mechanical reference

We have demonstrated the ability to determine position with 1 µm resolution and 10 µm accuracy over 1.6-m distances.

Variation in X Values
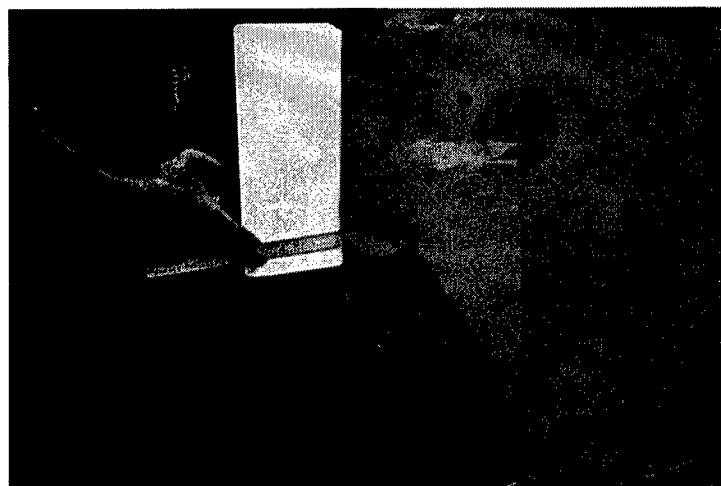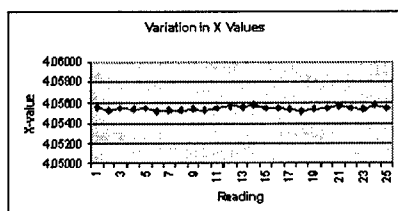
60 cm off axis parabola, 1.5 meters off axis, tested with a single CGH that gives wavefront correction, and creates array of alignment marks, as shown above.

Figure 14. Demonstration of the use of holographic alignment marks for providing an alignment reference for aspheric optics.
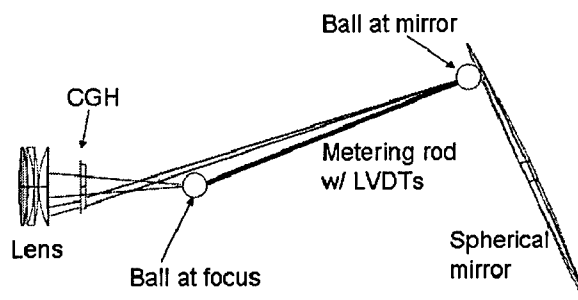
- Position a ball at focus of the 0th order diffraction beam after CGH, use it as a reference to position the spherical mirror.
- Use 4 tooling balls at the mirror surface, patches of CGH direct spherical beams toward the ball and the reflection fringes are used to position the balls accurately in lateral direction
- Metering rods are used to control the distance from the balls on the mirror to the ball at focus. The mirror is adjusted so that all the balls are at proper position.

Figure 15. Combination of laser metrology using a multiplexed CGH as reference and mechanical metering. With four such balls on the spherical mirror, its position and orientation can be determined to 5 µm.

(Plotted at a scale showing every 700 lines)

Null CGH for test of OAP
~20 µm pitch

Pattern for aligning CGH
to interferometer

Define position for tooling
ball at spherical mirror

Provides reference for
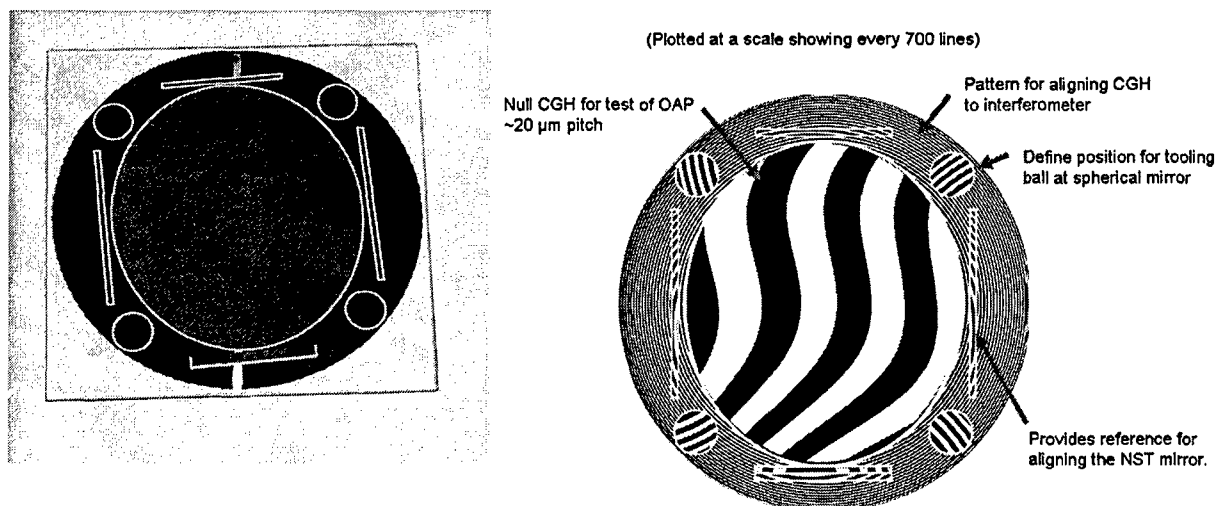aligning the NST mirror.

Figure 16. The CGH for the 1.7 m segment includes multiple patterns for alignment as well as wavefront correction. We show the layout of the different patterns as well as a photograph of a prototype multiplexed CGH.

5. Low-stress coatings for high-energy laser systems

The work of our program on optical coatings concentrated on three main areas: the development of negative thermal expansion (NTE) thin films, modeling the mechanical characteristics of optical coatings, and developing high-power adaptive optics structures. Several important advances were made, which will be discussed in turn. The most significant accomplishments are listed below:

1. First deposited NTE thin films

2. Successful analysis of films that determined that film density must be near the crystalline value to see NTE

3. Successful characterization of film mechanical properties

4. Numerical, predictive mechanical model of multilayer coatings on thin membranes

5. Load and deflection characterization of test coatings that closely match our models

6. Mechanically matched NTE coatings on zero-expansion mirror wafers

7. Investigations of heat transfer in micromachined adaptive mirrors that indicate air conduction, solid-state conduction, and transition regions

8. Design and initial processing of MEMS adaptive mirrors with enhanced heat transfer and very long throw

5.1 Negative thermal expansion thin films

One of the most exciting outcomes of our research is the development of the first NTE thin films. Since 1997, there has been a significant amount of research on bulk crystals of ZrW_2O_8, which shows strong NTE. However, prior to this program, no systematic way for preparing thin films of NTE material had been developed.

The reason that we began to explore NTE thin films was to stabilize the mechanical properties of optical coatings on arbitrary substrates. Of particular interest to the program were coatings on very thin zero-expansion glass such as would be used for space-based lightweight mirrors. Since all known optical

coating materials had positive thermal expansion, a negative material is needed to help stabilize the thermal properties of the system. NTE films would also be of particular benefit to lightweight polymer membrane mirrors, whose extreme thinness approaches the level of micromechanical mirrors.

Figure 17 shows a measurement of the coefficient of thermal expansion of a thin film on a cylindrically symmetric micromirror. The data were taken by examining the curvature change of the mirror as a function of temperature. The measurement was checked using a curvature measurement of an identical thin film on a bare silicon wafer and both were found to have similar NTE.
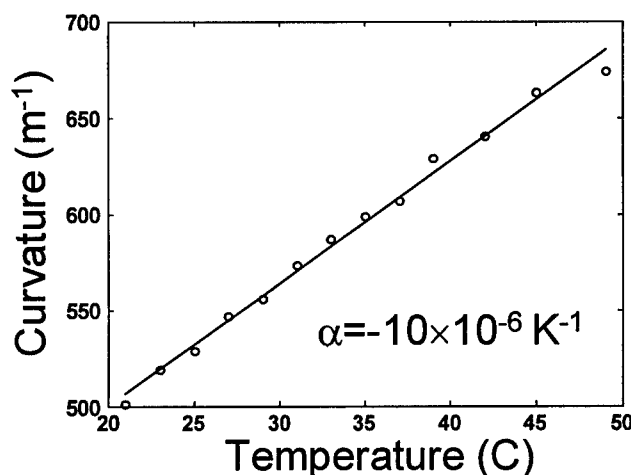
<figure>
Plot of Curvature (m^{-1}) versus Temperature (C). Data points rise approximately linearly from about 500 m^{-1} at 20 C to about 675 m^{-1} at 50 C, with a fitted straight line.

$\alpha = -10 \times 10^{-6}\ K^{-1}$
</figure>

Figure 17. Curvature vs. temperature for a Zr$_x$W$_y$O$_z$ coated micromirror. The NTE can be inferred from the rapidly increasing curvature in the upward direction.

The physics of the thin films may shed quite a bit of light on NTE in general. While the best known NTE materials are crystalline, thin films of Zr$_x$W$_y$O$_z$ are completely amorphous, as shown in Figure 18. Evaporated but not sputtered films show NTE. Further, they are non-stoichiometric, and we have found that depositing even pure WO$_3$ without Zr will lead to a NTE film under the right conditions. The common link among all of the materials and data appears to be closely related to density.

Our recent work with WO$_3$ suggests that common positive expansion oxides can be induced to take on NTE properties if the deposition conditions are right. If true for other oxides, then films near the bottom of a high reflectivity stack might be deposited for optimal mechanical properties while layers near the top can be deposited for lowest loss optical properties. In this way coatings could be simultaneous optimized for multiple properties at once with fewer trade-offs using standard materials. Exploring this will be one of our major goals for Years 4 and 5.
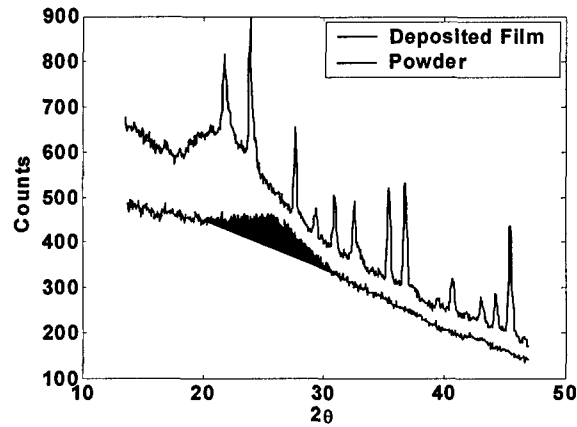
Figure 18. X-ray diffraction measurements of crystalline $Zr_xW_yO_z$ powder and amorphous thin films. The lack of X-ray peaks in the lower curve clearly indicates that the thin film has no crystalline structure.

5.2 Mechanical modeling of HEL coatings

Another goal of the program was to tackle the very difficult problem of modeling the optomechanical properties of optical coatings on thin mirrors. The desired output includes maps of deformation, stress, and temperature distribution. As part of this effort, we have fabricated optical coating membranes with integrated sensors to create temperature and strain maps across the coatings when they are stressed by external loads or high-power illumination. (Note that the sensors are *underneath* the coating and thus are nor directly excited by the light.) Presently, we have models in place for planar mirrors and are testing them with our sensor-embedded mirrors. Some of the early data are shown in Figure 19 and show very strong agreement. The properties of our NTE thin films have also been incorporated into the modeling. We plan to extend our models to non-planar mirror surfaces and polymer membrane mirrors.
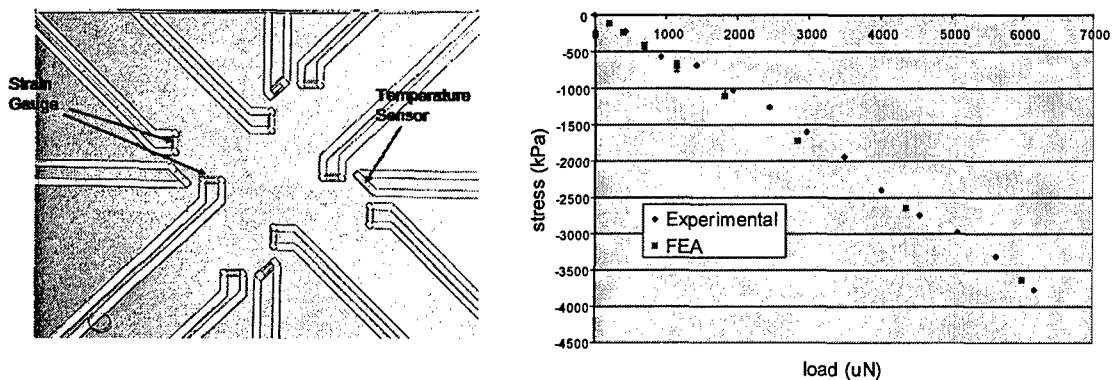

Figure 19. Embedded strain sensors (left) and match with data from our coating theoretical models (right). Note that the sensors are underneath the coatings and are thus do not impact the mirror's interaction with the light. The experimental plot shown is film stress as a function of mechanical load. The modeling has been performed using finite element methods.

21

5.3 Enhanced heat transfer and large throw in HEL adaptive optics

Another advance that we pursued in this program is adaptive micro-optics for HEL mirrors with enhanced heat transfer and large throw. The basic mirror uses a piston drive and is composed of a continuous face-sheet with hollow pistons extending down from the membrane, one for each mirror actuator as shown in Figure 20. This design concept is significantly different from present research in the area in that the spacing between pairs of electrodes is very small. This enhances the heat transfer and allows actuation at relatively low voltages. Further, the actuators use principles similar to those in comb drives for micropositioning, allowing a very large throw. We expect about a 4-fold increase in heat handling capabilities and a travel range of 20-30 μm with good speed. These numbers are significantly better than the state of the art and would enable the use of such mirrors for HEL and aero-optics.
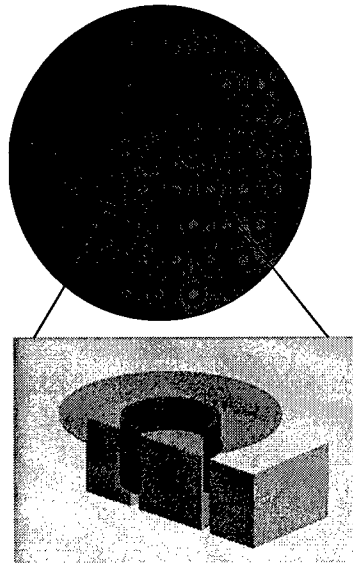

Figure 20. Conceptual diagram of actuator. The upper drawing shows a bird's-eye view of the continuous face sheet with cylindrical piston in red (not to scale). The lower drawing shows a cylindrical cut-away of the actuator with the cylinder sliding into a sheath in the silicon substrate. Up and down actuation operates on similar principles to an electrostatic comb-drive (electrodes not shown).

Figure 21 shows the result of some of the early processing. The devices show strong bonding and good deep reactive ion etch characteristics.

Long throw piston

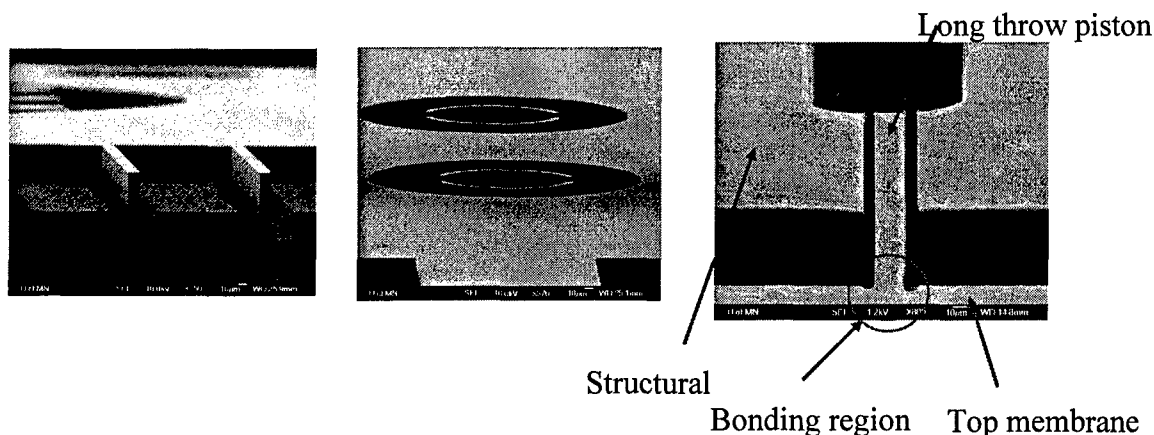Structural

Bonding region   Top membrane

Figure 21. SEM photos of early processing of piston-drive adaptive optics. The left image shows the quality of our deep trench processing, the middle image shows the cylindrical actuators prior to bonding of the top membrane, and the right image shows an actuator after bonding. This actuation approach significantly improves the state of the art for travel range and heat transfer while maintaining low control voltages.

6. Publications

1. M. S. Sutton and J. J. Talghader, "Zirconium tungstate based micromachined negative thermal expansion thin films," submitted to IEEE Journal of Microelectromechanical Systems, Oct. 2003.

2. M. S. Sutton and J. J. Talghader, "Micromachined negative thermal expansion thin films," Transducers 2003 Digest of Technical Papers, pp. 1148-1151, June 8-12, 2003, Boston, MA.

3. H. M. Martin, J. H. Burge, B. Cuerden, S. M. Miller, B. Smith and C. Zhao, "Manufacture of 8.4 m off-axis segments: a 1/5-scale demonstration", Optical Fabrication, Metrology, and Material Advancements for Telescopes, ed. E. Atad-Ettedgui and P. Dierickx, SPIE 5494, p. 62 (2004).

4. F. Y. Pan, J. H. Burge, R. Zehnder and Y. Wang, "Fabrication and alignment issues for segmented mirror telescopes," Applied Optics 43 (13), 2632-2642 (2004).

5. F. Y. Pan and J. H. Burge, "Efficient testing of segmented aspherical mirrors using a reference plate and computer generated holograms. 1: Theory and system optimization", accepted for publication in Applied Optics.

6. F. Pan, J. Burge and D. Anderson, "Efficient testing of segmented aspherical mirrors using a reference plate and computer generated holograms. 2: Experimental validation, case study and error analysis," accepted for publication in Applied Optics.

Presentations at technical conferences:

1. C. Zhao, R. Zehnder, and J. H. Burge, "Testing an off-axis parabolic mirror with a CGH and a spherical mirror as null lens," SPIE Annual meeting, Denver August 2004.

2. J. H. Burge , "Metrology Challenges for Next Generation Telescopes," Astronomical Telescopes and Instrumentation, SPIE Glasgow June 2004.

3. J. H. Burge, J. Sasian, H. M. Martin, R. Zehnder, C. Zhao, "Interferometric metrology for the Giant Magellan Telescope primary mirror," Astronomical Telescopes and Instrumentation, SPIE Glasgow June 2004.

REPORT DOCUMENTATION PAGE

AFRL-SR-AR-TR-06-0192

1. REPORT DATE (DD-MM-YYYY)	2. REPORT TYPE	3. DATES COVERED (From - To)
25-05-2006	final report	15-07-2002 – 15-07-2005

4. TITLE AND SUBTITLE	5a. CONTRACT NUMBER
Fabrication, Testing, Coating and Alignment of Fast Segmented Optics	
	5b. GRANT NUMBER
	F49620-02-1-0384
	5c. PROGRAM ELEMENT NUMBER

6. AUTHOR(S)	5d. PROJECT NUMBER
Hubert Martin, Roger Angel, James Burge, Joseph Talghader	F496200210384
	5e. TASK NUMBER
	5f. WORK UNIT NUMBER

7. PERFORMING ORGANIZATION NAME(S) AND ADDRESS(ES)	8. PERFORMING ORGANIZATION REPORT NUMBER
Steward Observatory University of Arizona Tucson, AZ 85721	

9. SPONSORING / MONITORING AGENCY NAME(S) AND ADDRESS(ES)	10. SPONSOR/MONITOR'S ACRONYM(S)
Air Force Office of Scientific Research	AFOSR
801 N Randolph St Arlington, VA 22203-1977	11. SPONSOR/MONITOR'S REPORT NUMBER(S)

Dr Charles Lee

12. DISTRIBUTION / AVAILABILITY STATEMENT

Approve for Public Release: Distribution Unlimited

13. SUPPLEMENTARY NOTES

14. ABSTRACT
The report presents the results of the MRI addressing four of the most critical technologies needed to produce large-aperture, lightweight, high-power HEL systems. They are:
1. polishing large off-axis segments of fast primary mirrors;
2. testing large segments in an off-axis geometry;
3. alignment of multiple segments of a large mirror; and
4. coatings that reflect high-intensity light without distorting the substrate.
The program made substantial progress in all areas. Some of the most important results are the manufacture of a 1.7 m off-axis mirror segment; demonstration of new, powerful measurement techniques using computer-generated holograms; and the first-ever thin-film coating with negative thermal expansion.

15. SUBJECT TERMS

16. SECURITY CLASSIFICATION OF:			17. LIMITATION OF ABSTRACT	18. NUMBER OF PAGES	19a. NAME OF RESPONSIBLE PERSON
a. REPORT	b. ABSTRACT	c. THIS PAGE			Hubert Martin
				19	19b. TELEPHONE NUMBER (include area code) 520-621-9582

Standard Form 298 (Rev. 8-98)
Prescribed by ANSI Std. Z39.18